Synthetic Metals 212 (2016) 154–160

Contents lists available at ScienceDirect

Synthetic Metals

journal homepage: www.elsevier.com/locate/synmet

Removal of Hg (II) from aqueous solution using polypyrrole/SBA-15 nanocomposite: Experimental and modeling

Mina Shafiabadi[a], Ali Dashti[a,*], Habib-Allah Tayebi[b]

[a] Chemical Engineering Department, Faculty of Engineering, Ferdowsi University of Mashhad, Mashhad, Iran
[b] Department of Textile Engineering, Qaemshahr Branch, Islamic Azad University, Qaemshahr, Iran

ARTICLE INFO

Article history:
Received 20 October 2015
Received in revised form 7 December 2015
Accepted 23 December 2015
Available online xxx

Keywords:
Polypyrrole
SBA-15
Nanocomposite
Hg (II) ion
Adsorption

ABSTRACT

A nanocomposite of polypyrrole (PPy)/SBA-15 was synthesized, characterized and used for Hg (II) adsorption from aqueous medium. The adsorbent characterization was carried out using Fourier-transform infrared spectra (FT-IR), X-ray diffraction (XRD), N_2 adsorption/desorption, scanning electron microscopy (SEM) and transmission electron microscopy (TEM). Atomic absorption spectrophotometer (AAS) was also applied to determine the amount of Hg (II) ion in the solution. Effective parameters on Hg (II) removal such as pH, the amount of adsorbent and contact time were examined and optimized at temperatures ranging from 25 to 45 °C. Optimum values were pH 8, contact time of 60 min and the amount of absorbent of 1 g/l. The Langmuir and Freundlich adsorption isotherm models were applied and the presented results show very good agreement with Langmuir adsorption isotherm with high adsorption capacity of 200 mg/g. In addition, pseudo-second order kinetic equation was best fitted for adsorption kinetic model. The adsorption process data verified its spontaneous and endothermic nature.

1. Introduction

Nowadays, environmental pollution of heavy metals is a serious problem all over the world. Heavy metals are non-biodegradable and could easily enter into food chain through accumulation of living organisms. Toxic heavy metals such as Zn, Cu, Ni, Hg, Cd, Pb and Cr are the most concerning ions particularly in wastewater treatment industries result in soil and water contaminations [1].

For example, US environmental protection agency (EPA) specified maximum contaminant level (MCL) of mercury in drinking water about 0.002 mg/l (2 ppb) [2,3].The allowed limit of mercury in water is lower than other toxic heavy metal ions. Therefore, mercury removal from industrial wastewater and urban water is crucial [4]. Different methods such as adsorption, membrane filtration, chemical oxidation, ion exchange and precipitation have been introduced for toxic pollutants removal from industrial wastewater.

At present, the adsorption process is known as techno-economic approach to remove heavy metals and toxicants from aqueous solutions [1]. The selection of adsorbent with higher sorption capacity, more selectivity and lower-cost is the most important issue in adsorption process. Different kinds of adsorbents are: seaweeds, zeolites, activated carbon and mesoporous adsorbents like Al_2O_3 and silicates [1,5,6]. Mesoporous M41S silicate group including MCM-41 and SBA-15 is considered as suitable adsorbent due to high surface area, high pore volume and ordered structure to functionalize its surface [7–10].

The promising features of conductive polymers to hybrid with inorganic mesoporous materials improve their selectivity and relatively high metal adsorption capacities. Thus, these composite polymeric materials could use extensively for heavy metal removal from aqueous solutions [11,12]. Among them, polyaniline (PAni) and polypyrrole (PPy) were widely provided as adsorbents because of good environmental stability, low cost and ease of preparation.

The removal of Hg(II) ions from aqueous media using PAni and its nanocomposite was investigated by Ghorbani et al. [13]. Tang at al. [14]. synthesized novel PAni/SBA-15 nanocomposite and suggested the pseudo-second-order model for chemical process of adsorption kinetics.

The nanofiber of PPy–PAni used for adsorption of Cr (VI) from aqueous solution by Bhaumik et al. [6]. The Langmuir isotherm was the best fitting model in their adsorption process. Azioune et al. [15] used PPy powder and PPy-silica composite as a bioadsorbent for a model protein called human serum albumin (HSA). The nanocomposite of PPy and sawdust was prepared by Pahlavanzadeh et al. [16] to nitrate removal from aqueous media. The Freundlich isotherm was very good model for mentioned adsorption process. Hasani and Eisazadeh [17] investigated PPy and its

* Corresponding author. Fax: +98 51 38816840.
E-mail address: dashti@um.ac.ir (A. Dashti).

http://dx.doi.org/10.1016/j.synthmet.2015.12.020
0379-6779/

Al_2O_3 nanocomposite (with and without PVA as surfactant) to remove Cd (II) ion from aqueous solution. The Langmuir isotherm was well fitted in their equilibrium data. Lim et al. [18] examined PPy/colloidal silica nanocomposite to remove heavy metal ions such as Hg^{2+}, Ag^{+}, and Pb^{2+} from aqueous solution. They reported relatively high adsorption capacities of this nanocomposite material for heavy metals extraction. The modified PPy/MCM-41 nanocomposite synthesized by Javadian and Taghavi [19] showed high adsorption capacity for Hg (II) ion and the equilibrium data well fitted by Freundlich isotherm. For the first time, Cheng et al. [20,21] synthesized and characterized PPy nanocomposites with mesoporous silica including MCM-41 and SBA-15 nanocomposite. They investigated the electrorheology (ER) behavior of prepared nanocomposites. Cheng et al. [21] found the PPy/SBA-15 shows better ER performance the MCM-41 nanocomposite. Mehdinia et al. [22] used molecularly imprinted PPy based on SBA-15 for ascorbic acid adsorption. The results showed that the imprinted nanocomposites represented high selectivity and high adsorption for ascorbic acid adsorption.

Literatures reviews showed that few researchers applied PPy/SBA-15 nanocomposite to removal heavy metal ions from aqueous solutions particularly mercury removal. In this article, PPy/SBA-15 nanocomposite is synthesized, characterized and applied to study adsorption capacity of Hg (II) ion from aqueous by achieving optimum experimental conditions. The main novelty of this work is to present considerable potential of PPy/SBA-15 nanocomposite for the removal of Hg (II) from aqueous solution with higher adsorption capacity. Most of the important previous researches focused to electrorheology properties of PPy/SBA-15 [20,21], PPy/MCM-41 [23] or PAni/SBA-15 [24]. Recently, Javadian and Taghavi [19] carried out mercury removal using PPy/MCM-41 adsorption. The PPy/SBA-15 could achieve higher adsorption capacity than PPy/MCM-41 as expected and our data confirmed that q_m is about 200 mg/g compared to 164 mg/g for PPy/MCM-41 adsorbent system [19].

2. Experimental

2.1. Materials

Pluronic P123 surfactant (EO20PO70EO20, $M_w = 5800$), tetraethylorthosilicate (TEOS, 98%), pyrrole (distilled before use) and $FeCl_3{\cdot}6H_2O$ was used as initiator for polymerization of pyrrole. Standard solution of Hg (II) (1000 mg/l) was prepared by dissolving 0.171 g of Hg $(NO_3)_2$ in 100 ml of distilled water. Other chemical materials were received purely and purchased from Merck Co.

2.2. Mesoporous SBA-15 synthesis

Mesoporous SBA-15 was synthesized according to Zhao et al. [25] as following: 12.5 ml of P123 as surfactant and 375 ml of distilled water along with 75 ml (0.1 N) of HCl were stirred at 42 °C. Then, 31.5 ml of TEOS as the silica source was added to the homogeneous mixture. The obtained gel was placed in static conditions at 42 °C for 24 h. Next, the temperature was increased to 138 °C and maintained for 24 h. After filtration, the obtained powder was transferred to a furnace for calcinations at 550 °C for 5 h in order to remove existing organics in its pores.

2.3. Synthesis of PPy/SBA-15 nanocomposite

For the synthesis of PPy/SBA-15 nanocomposite, 5.4 g of $FeCl_3$ was dissolved into 100 ml of distilled water and stirred for 20 min. Then, 1 gr of SBA-15 and 1 ml pyrrole were added to the filtered solution and the product was stirred for 5 h to complete polymerization. Finally, the product was filtrated and dried in oven for 24 h.

2.4. Instrumentation

Low angle X-ray spectra patterns in the range of 0.6–9 were determined with XPERT-PRO40 kV spectrometer using Cu Kα radiation (λ = 1.5406 Å). FT-IR results were recorded via Shimadzu 4300 Fourier transform infrared spectroscopy. N_2 adsorption/desorption isotherms were carried out on Chem BET 3000 TPR/TDP, USA at 77 K. TEM images were taken by Philips, CM/20, Netherlands. SEM images were obtained using a TESCAN MIRA3 microscope.

2.5. Adsorption experiments

Batch experiments were carried out through contacting 100 mg of PPy/SBA-15 with 100 ml Hg (II) solution with different initial concentrations at various pH values and temperatures of 25, 35 and 45 °C. The pH values of the solution were adjusted in the range of 2–12 using 0.1 N solutions of HCl and NaOH. The products were placed in a shaker with 200 rpm velocity for 2 h in order to accomplish adsorption process. At the end of the process, the adsorbent was separated by centrifuging at 4000 rpm in 20 min. The amount of mercury in the solution before and after adsorption process was measured by atomic adsorption spectrometer (AAS) as PerkinElmer Corp model 2380. Mass balance was applied for calculating the amount of adsorbed Hg (II) by PPy/SBA-15 nanocomposite.

3. Results and discussion

3.1. Characterization analyses

The N_2 adsorption/desorption isotherms of SBA-15 and PPy/SBA15 nanocomposite are shown in Fig. 1. The SBA-15 sample exhibits isotherm of type IV according to the IUPAC nomenclature with a hysteresis loop of type H_1 and a steep increase of adsorbed N_2 at relative pressure $P/P_0 = 0.6–0.8$ as expected for mesoporous materials [20,21,23–25]. Also, the BJH pore size distribution curve showed the presented SBA-15 has narrow pore size distribution with average pore size of 8.2 nm.

In Table 1, the specific BET surface area, pore volume and average pore diameter of SBA-15 and PPy/SBA-15 nanocomposite calculated from N_2 adsorption isotherms using the BJH method are summarized.

In the case of PPy/SBA-15, after polymerization of pyrrole chains, the inflection point of the isotherm shifts to lower

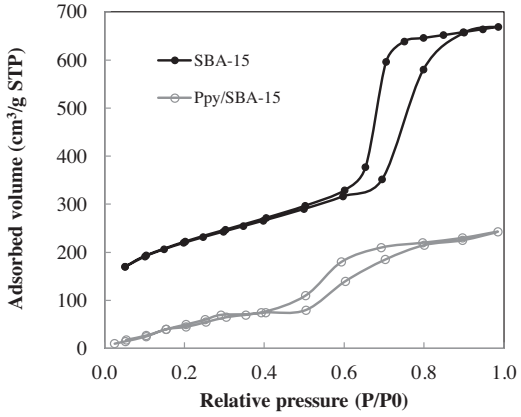

Fig. 1. N_2 adsorption/desorption isotherms of SBA-15 and PPy/SBA-15.

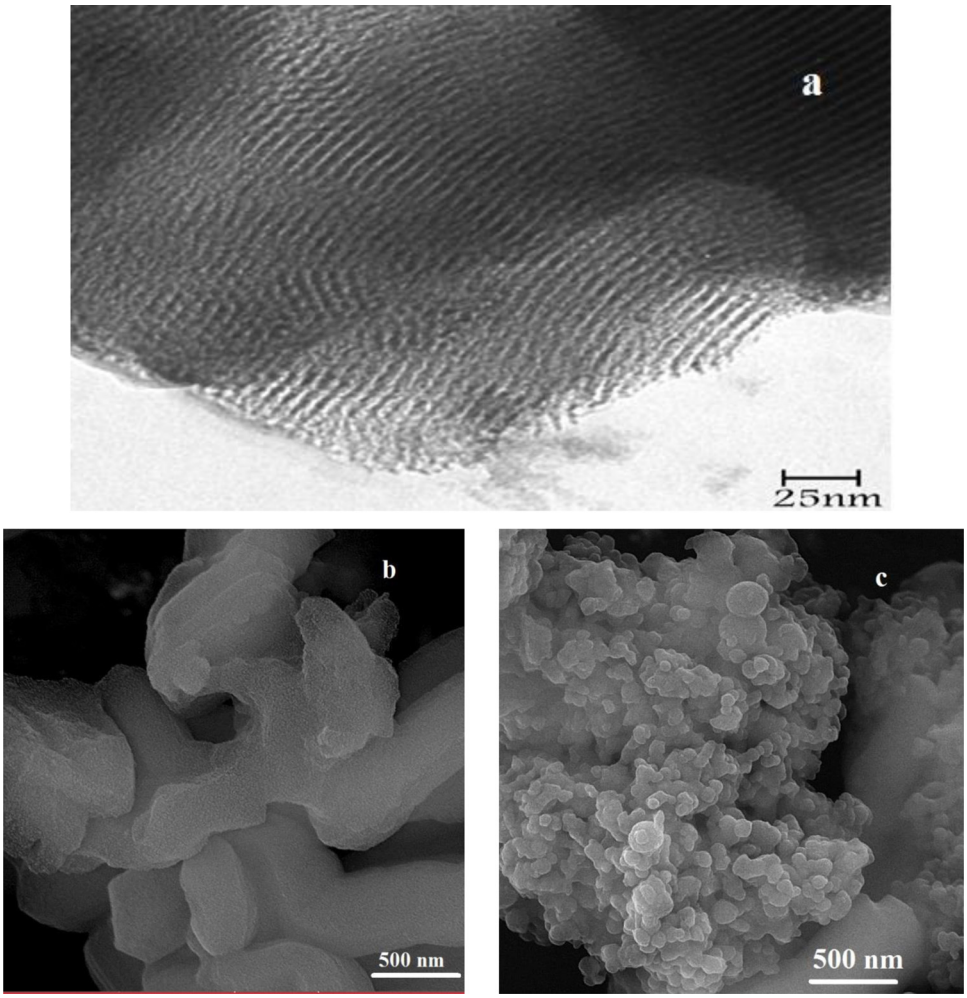

Fig. 2. Morphology images of (a) TEM of SBA-15 (b) SEM of SBA-15 and (c) SEM of PPy/SBA-15 nanocomposite.

P/*P*0 which supports that PPy actually inserted inside the channels of SBA-15 [21,24]. In addition, the decrease in BET surface area, mesopore volume and pore size of PPy/SBA-15 nanocomposite clearly indicates that the polymer well incorporated into the channels of SBA-15 [21,23,24].

Morphology of synthesized SBA-15 was characterized by TEM equipment. Fig. 2a exhibits TEM image with the electron beam parallel to the direction of main channels of SBA-15. The SBA-15 shows hexagonal well-ordered mesoporous structure which already found by Cheng et al. [20]. The pore size diameter of SBA-15 can be estimated about 7–8 nm which is close to the pore size calculated by BJH method.

Furthermore, SEM images of SBA-15 and PPy/SBA-15 nanocomposite are shown in Fig. 2b and c, respectively. According to Fig. 2c, the PPy polymerization was occurred not only insides the pores, but also the outside the SBA-15. Thus, this event could further support the lower surface area of PPy/SBA-15 than SBA-15 as reported in Table 1.

Low Angle XRD patterns of synthesized SBA-15 and PPy/SBA-15 samples for $0 < 2\theta < 10$ is shown in Fig. 3. The XRD analysis Exhibits 3 peaks: one strong peak (1 0 0) at 0.95°, corresponding d spacing is 9.3 nm, and two weak peaks (1 1 0) and (2 0 0) at 1.59° and 1.81° respectively, which represent hexagonal structure of

Table 1
Characteristics of SBA-15 and PPy/SBA-15 samples.

Sample	Surface area (BET) (m^2/g)	Pore diameter (BJH) (nm)	Pore volume (BJH) (cm^3/g)
SBA-15	743.5	8.2	0.98
PPy/SBA-15	97.6	3.1	0.22

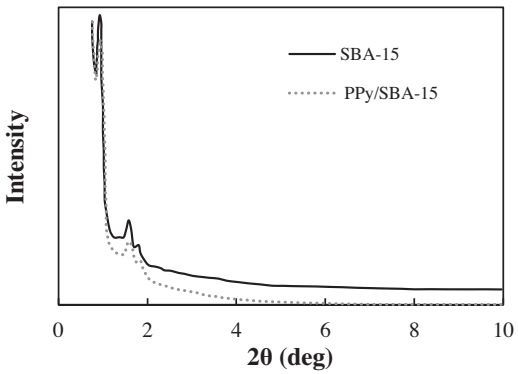

Fig. 3. Low angle XRD patterns of SBA-15 and PPy/SBA-15.

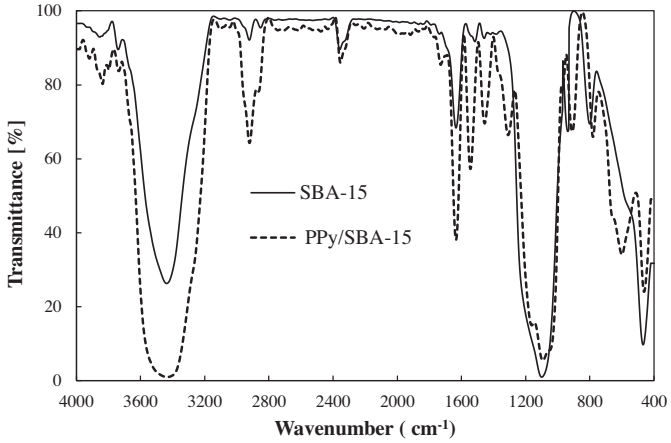

Fig. 4. FT-IR spectra of SBA-15 and PPy/SBA-15.

synthesized silicate mesoporous material [26]. After PPy insertion into SBA-15 pores, the XRD pattern has not changed. However, observed significant reduction of peak intensities for PPy/SBA-15 could be related to fill out channels of SBA-15 pores by PPy polymers [23,24,27]. In addition, the decrease in BET surface area, mesopore volume and pore size of PPy/SBA-15 nanocomposite clearly indicates that the polymer well incorporated into the channels of SBA-15 [21,23,24]. The approximate pore size of SBA-15 calculated by the BJH formula, 8.2 nm as reported in Table 1, is smaller than the d spacing 9.3 nm for plane (1 0 0) of XRD pattern, since XRD includes also thickness of silica walls [25].

The FT-IR spectra of SBA-15 and PPy/SBA-15 are shown in Fig. 4. In SBA-15, the bands 788 and 1099 cm^{-1} belong to the symmetrical vibrations and anti-symmetric of bond Si—O—Si. The peaks at 466, 935 and 3434 cm^{-1} are attributed to the torsion vibration of the bond Si—O—Si and the vibration of the Si—OH group, respectively. These peaks are assigned to SBA-15 frame work and can also be seen in the spectra of PPy/SBA-15.

In PPy/SBA-15, the strong broad band at 3427 cm^{-1} can be attributed to stretching vibrations of PPy or to single bridge compounds polymeric association. The bands at 2918 and 2356 cm^{-1} refer to the stretching vibration of C—H bond and C—N stretching vibration, respectively. The absorption band at 1635 cm^{-1} was assigned to the C=C ring stretching of pyrrole. The band at 1305 cm^{-1} is due to C—H vibrations. The peak at 1091 cm^{-1} corresponds to the in-plane deformation of O—H group and C—O symmetric stretching. The peak at 910 cm^{-1} could

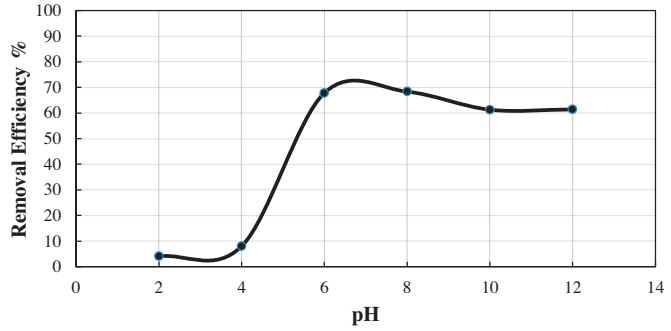

Fig. 5. Effect of pH on Hg (II) removal (100 ml of 60 mg/l Hg (II), time = 2 h, T = 25 °C and the amount of adsorbent = 100 mg).

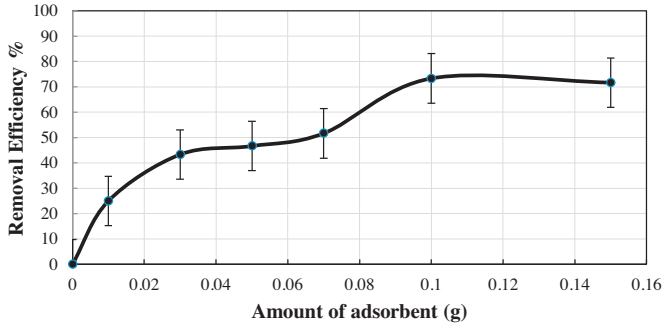

Fig. 6. Effect of adsorbent PPy/SBA-15 amount on Hg (II) adsorption (100 ml of Hg (II) solution with 60 mg/l concentration at 25 °C and pH 8).

be assigned to the C—H deformation vibration in the CH=CH group [21,22,27,28]. In SBA-15 FT-IR pattern compared with PPy/SBA-15, some of bands have been disappeared which indicates incorporation of PPy chains with SBA-15 particles.

3.2. Adsorption studies

3.2.1. Effect of pH

One of the important parameters in adsorption process is pH of the solution to control amount of metal ions at adsorbent sites [29]. The adsorption capacity was examined by varying pH ranging from 2 to 12 while other parameters such as the amount of PPy/SBA-15 adsorbent, concentration of metal ions and temperature remain constant. The effect of pH changes on removal efficiency of Hg (II) ion is shown in Fig. 5. The initial concentration of metal and the amount of adsorbent were 60 mg/l and 0.1 g, respectively.

The metal adsorption increases while increasing pH from 4 to 8, and then decreases. According to Fig. 5, the removal efficiency is 8% at pH 4 and reaches to about 68.3% at pH 8.0. At low pH values it may probable to protonation of adsorbent surface [9]. which causes the exclusion of Hg^{2+} ions. Also, because of high concentration of H^+ ions in lower pH, it may compete with metal ions in adsorbent active sites. As pH increases, the competition between H^+ ions and Hg^{2+} ions at adsorbent active sites reduces, result in increasing capacity adsorption [9]. Further increasing of pH value, the metal species in the solution change in other ways and enhancing heavy metal removal is been attributed to reduction in solubility and precipitation of solid metal hydroxide [9]. Therefore, no more adsorption occurs with formation of Hg $(OH)_2$ at higher values of pH.

3.2.2. Effect of adsorbent dosage

The effect of adsorbent PPy/SBA-15 amount was investigated ranging from 0.01 to 0.15 g at pH 8.0 in 100 ml solution with 60 mg/l Hg (II) ion concentration. The obtained results are presented in Fig. 6. By increasing adsorbent dosage to 0.1 g, removal efficiency would enhance as expected. At 0.1 g value, the maximum efficiency is about 73.3%. However, further addition of adsorbent does not affect removal efficiency probably due to adsorbent particles aggregation [30,31]. Therefore, 1 g/l of nanocomposite is demonstrated as optimum adsorbent quantity to Hg (II) removal in this study.

3.2.3. Effect of contact time and temperature

Adsorption of Hg (II) ion using PPy/SBA-15 adsorbent as a function of contact time was investigated in three different temperatures at 25, 35 and 45 °C. The obtained results were demonstrated in Fig. 7. It can be observed that at initial stage of adsorption, mercury removal has faster rate due to more active sites accessibility and then gradually slower rate until the

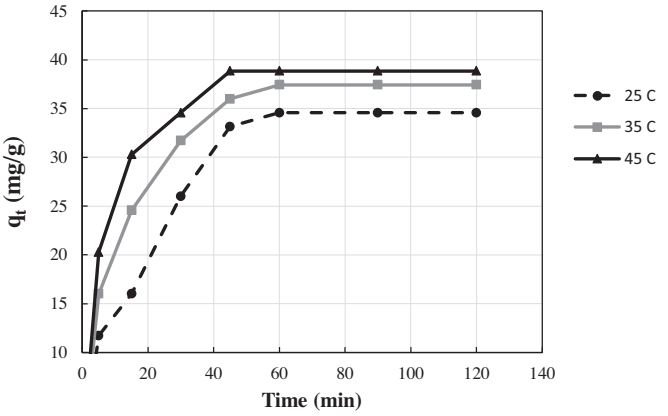

Fig. 7. Effect of adsorption contact time of Hg (II) ion at different temperatures 25, 35, 45°C (100 ml Hg (II) solution with 40 mg/l concentration, 100 mg of PPy/SBA-15 at pH 8).

equilibrium is achieved at 60 min when adsorption sites become filled out [32]. As shown in Fig. 7, amount of adsorbate per unit mass of adsorbent at time t (mg/g), q_t, increases by increasing temperature from 25 to 45 °C indicating endothermic nature of adsorption process as discussed later. However, the simple, safe and tech-economical way is to perform experiments at room temperature without considerable decrease of adsorption efficiency.

3.3. Adsorption isotherm

Adsorption isotherm represents the interaction between adsorbent and adsorbate and this study is required for designing adsorption systems. In order to investigate Hg (II) adsorption, experimental data were studied with 0.1 g of PPy/SBA-15 adsorbent at optimum pH 8 and 25 °C. Two most popular isotherms including Freundlich and Langmuir models were applied to explore Hg (II) adsorption in our study. The Freundlich isotherm is an empirical model is generally used for describing heterogeneous systems [33]. The Langmuir isotherm is based on monolayer adsorption onto adsorbent surface and adsorption occurs at identical homogeneous sites of the adsorbent surface without any interaction between adsorbate molecules [34]. Linear form of the Langmuir and Freundlich isotherms are presented by equations 1 and 2 respectively:

$$\frac{C_e}{q_e} = \frac{C_e}{q_m} + \frac{1}{bq_m} \quad (1)$$

$$\ln q_e = \ln K_f + \frac{1}{n}\ln C_e \quad (2)$$

where q_e is the equilibrium adsorption capacity of the adsorbent (mg/g), C_e is the equilibrium concentration (mg/l), q_m is the maximum monolayer adsorption capacity (mg/g), b is the Langmuir constant related to the energy of adsorption (l/mg), K_f is the adsorption capacity of the adsorbent and n is the empirical constant for intensity of adsorption related to adsorbent heterogeneity. In adsorption process, the higher amounts of n are desirable [35]. The mentioned isotherm models were plotted for adsorption data at 25 °C and model parameters were calculated and presented in Table 2. As presented, the Langmuir model fits the data better than Freundlich model. It can be seen from Table 2 that the maximum amount of Hg (II) adsorption using PPy/SBA-15 adsorbent is 200 mg/g whereas for other adsorbents like SWCNTs (single-walled carbon nanotubes) is about 25.6 mg/g as reported by Yaghmaeian et al. [36]. In addition, for further evaluation a listed of adsorbents and their adsorption capacity for Hg removal was presented by Zabihi et al. [37].

3.4. Adsorption kinetics

To finding which mechanism (diffusion or reaction) is predominately as limiting-step in adsorption process, different kinetic models have been used to evaluate experimental data. Commonly, pseudo-first and pseudo-second linear kinetic models, as stated by equations 3 and 4 respectively, were used to fit the kinetic data:

$$\ln(q_e - q_t) = \ln q_e - tk_1 \quad (3)$$

$$\frac{t}{q_t} = \frac{1}{k_2 q_e^2} + \frac{t}{q_e} \quad (4)$$

where q_t is the amount of adsorbate per unit of adsorbent at time t (mg/g), k_1 and k_2 are pseudo-first order and pseudo-second order rate constants, respectively. Rate constants and adsorption capacities for pseudo-first order from best fitting obtained from plotted $\ln(q_e - q_t)$ versus t data and for pseudo-second order from plotted t/q_t versus t data were estimated and corresponding values are reported in Table 3. The kinetic of adsorption of Hg (II) with PPy/SBA-15 is described well by pseudo-second order model. The calculated value of q_e from pseudo-second order model is closer to the experimental value ($q_{e,exp}$ = 34.57). Therefore, adsorption kinetic of Hg (II) with PPy/SBA-15 adsorbent is better described by pseudo-second order kinetic model.

The rate limiting-step can be single or a combination of diffusion steps. Usually, intra-particle diffusion is the rate limiting-step as given by Weber and Moriss [38]. presented by equation 5 as following:

$$q_t = k_{id} t^{1/2} + C_{st} \quad (5)$$

where, k_{id} is intra-particle rate constant (mg/g/min$^{0.5}$). The plot of q_t versus $t^{0.5}$ is depicted to predict the rate limiting-step. From Fig. 8, it can be seen that the adsorption of Hg (II) ion is consisted of a few linear plots. The first section of the plot is because of the boundary layer diffusion and deviation from the center indicates boundary layer thickness, then at second section of the plot, adsorption reduction is attributed to the intra-particle diffusion mechanism [2,38]. For intra-particle diffusion model, estimated values of rate constant k_{id} and R_1^2 by data regression are 4.912 and 0.97 respectively.

Table 2
Langmuir and Freundlich isotherm parameters for Hg (II) ion with PPy/SBA-15 adsorbent.

Langmuir isotherm			Freundlich isotherm		
q_m (mg g^{-1})	b(l mg^{-1})	R^2	K_f(mg/g(L/mg)$^{1/n}$)	N	R^2
200	0.004	0.993	2.32	1.48	0.985

Table 3
Pseudo-first order and pseudo-second order model parameters for Hg (II) ion adsorption by PPy/SBA-15 adsorbent.

pseudo-first order			pseudo-second order		
k_1 (min^{-1})	q_e (mg/g)	R^2	k_2 (mg/g min)	q_e (mg/g)	R^2
0.04	30.05	0.958	0.0017	40	0.986

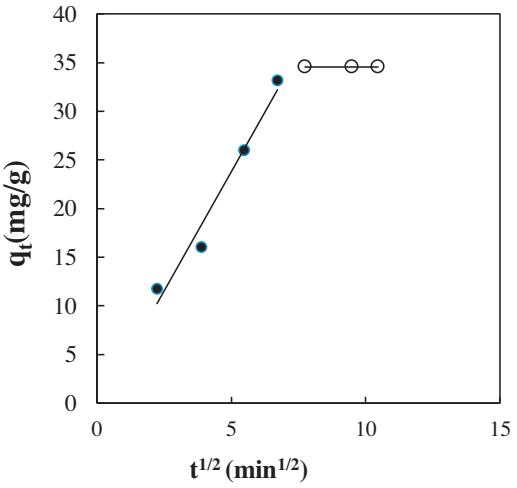

Fig. 8. Kinetic diagram for Hg (II) ion removal by PPy/SBA-15 adsorbent.

3.5. Adsorption thermodynamics

Thermodynamic analysis is applied to understand the nature and mechanism of adsorption process. ΔG, ΔH and ΔS values are calculated from equations 6 and 7 to describe thermodynamic behavior of adsorbate:

$$\Delta G = -RT\ln k_d \quad (6)$$

$$\ln k_d = \frac{\Delta S}{R} - \frac{\Delta H}{RT} \quad (7)$$

where, ΔH (J/mol) and ΔS (J/mol.K) are predicted from slope and intercept of data plotting of ln (k_d) versus 1/T. The thermodynamic parameters are reported in Table 4. The negative ΔG values confirm the spontaneous nature of Hg (II) adsorption. The ΔG values are in the range −20 to 0 kJ/mol which indicates Hg (II) adsorption is a physisorption process [39]. Moreover, positive values of ΔH for Hg (II) ion represent its endothermic nature. The positive value of ΔS indicates the reversible adsorption of Hg (II) ion with PPy/SBA-15 nanocomposite.

4. Conclusions

In the present study, PPy/SBA-15 nanocomposite was synthesized, characterized and applied for Hg (II) ion adsorption from aqueous solution in batch media. Optimal conditions of Hg (II) removal was obtained at pH 8, contact time of 60 min and absorbent dosage of 1 g/l at room temperature. The experimental data were fitted well by Langmuir model and the maximum adsorption capacity was estimated to be 200 mg/g. Hg (II) ion adsorption followed the pseudo-second order kinetic model. Results showed that PPy/SBA-15 nanocomposite is an appropriate adsorbent for Hg (II) ion removal from aqueous media. Thermodynamical investigation presented the endothermic nature and physisorption mechanism of mercury removal by PPy/SBA-15 nanocomposite.

Table 4
Thermodynamic parameters of adsorbed Hg (II) by PP/SBA-15 nanocomposite.

ΔH (kJ/mol)	ΔS (J^{-1} mol^{-1} K^{-1})	ΔG (kJ/mol)			R^2
		298 K	308 K	318 K	
19.82	81.05	−3.93	−4.74	−5.55	0.989

References

[1] F. Fu, Q. Wang, Removal of heavy metal ions from wastewaters: a review, J. Environ. Manage. 92 (2011) 407–418.
[2] Basic Information about Mercury (inorganic) in Drinking Water, United States Environmental Protection Agency http://water.epa.gov/drink/contaminants/basicinformation/mercury.cfm.
[3] M. Anbia, Sh. Amirmahmoodi, Removal of Hg (II) and Mn (II) from aqueous solution using nanoporous carbon impregnated with surfactants, Arabian J. Chem. (2011) (in press) (corrected proof).
[4] R.K. Gupta, R.A. Singh, S.S. Dubey, Removal of mercury ions from aqueous solutions by composite of polyaniline with polystyrene, Sep. Purif. Technol. 38 (2004) 225–232.
[5] S. Babel, T.A. Kurniawan, Low-cost adsorbents for heavy metals uptake from contaminated water: a review, J. Hazard. Mater. B 97 (2003) 219–243.
[6] M. Bhaumik, A. Maity, V.V. Srinivasu, M.S. Onyango, Removal of hexavalent chromium from aqueous solution using polypyrrole-polyaniline nanofibers, Chem. Eng. J. 181–182 (2012) 323–333.
[7] Zh. Chen, L. Zhou, F. Zhang, Ch. Yu, Zh. Wei, Multicarboxylic hyperbranched polyglycerol modified SBA-15 for the adsorption of cationic dyes and copper ions from aqueous media, Appl. Surf. Sci. 258 (2012) 5291–5298.
[8] S.M. Rivera-Jiménez, S. Méndez-González, A. Hernández-Maldonado, Metal ($M = Co^{2+}$, Ni^{2+}, and Cu^{2+}) grafted mesoporous SBA-15: effect of transition metal incorporation and pH conditions on the adsorption of Naproxen from water, Microporous Mesoporous Mater. 132 (2010) 470–479.
[9] A. Shahbazi, H. Younesi, A. Badiei, Functionalized SBA-15 mesoporous silica by melamine-based dendrimer amines for adsorptive characteristics of Pb (II), Cu (II) and Cd (II) heavy metal ions in batch and fixed bed column, Chem. Eng. J. 168 (2011) 505–518.
[10] L. Mercier, T.J. Pinnavaia, Heavy metal ion adsorbents formed by the grafting of a thiol functionality to mesoporous silica molecular sieves: factors affecting Hg (II) uptake, Environ. Sci. Technol. 32 (1998) 2749–2754.
[11] B. Samiey, C. Cheng, J. Wu, Organic–inorganic hybrid polymers as adsorbents for removal of heavy metal ions from solutions: a Review, Materials 7 (2) (2014) 673–726.
[12] C. Sanchez, B. Julián, P. Belleville, M. Popall, Applications of hybrid organic–inorganic nanocomposites, J. Mater. Chem. 15 (2005) 3559–3592.
[13] M. Ghorbani, M. Soleimani Lashkenari, H. Eisazadeh, Application of polyaniline nanocomposite coated on rice husk ash for removal of Hg (II) from aqueous media, Synth. Metals 161 (2011) 1430–1433.
[14] R. Tang, Q. Li, H. Cui, Y. Zhang, J. Zhai, Adsorption of aqueous Hg (II) by a novel poly(aniline-co-o-aminophenol)/mesoporous silica SBA-15 composite, Polym. Adv. Technol. 22 (2011) 2231–2236.
[15] A. Azioune, K. Pech, B. Saoudi, M.M. Chehimi, G.P. McCarthy, S.P. Armes, Adsorption of human serum albumin onto polypyrrole powder and polypyrrole-silica nanocomposites, Synth. Metals 102 (1999) 1419–1420.
[16] H. Pahlavanzadeh, R. Katal, H. Mohammadi, Synthesize of polypyrrole nanocomposite and its application for nitrate removal from aqueous solution, J. Ind. Eng. Chem. 18 (2012) 948–956.
[17] T. Hasani, H. Eisazadeh, Removal of Cd (II) by using polypyrrole and its nanocomposites, Synth. Metals 175 (2013) 15–20.
[18] C.W. Lim, K. Song, S.H. Kim, Synthesis of PPy/silica nanocomposites with cratered surfaces and their application in heavy metal extraction, J. Ind. Eng. Chem. 18 (2012) 24–28.
[19] H. Javadian, M. Taghavi, Application of novel polypyrrole/thiol-functionalized zeolite Beta/MCM-41 type mesoporous silica nanocomposite for adsorption of Hg^{2+} from aqueous solution and industrial wastewater: kinetic, isotherm and thermodynamic studies, Appl. Surf. Sci. 289 (2014) 487–494.
[20] Q. Cheng, V. Pavlinek, C. Li, A. Lengalova, Y. He, P. Saha, Synthesis and characterization of new mesoporous material with conducting polypyrrole confined in mesoporous silica, Materi. Chem. Phys. 98 (2006) 504–508.
[21] Q. Cheng, V. Pavlinek, A. Lengalova, C. Li, Y. He, P. Saha, Conducting polypyrrole confined in ordered mesoporous silica SBA-15 channels: preparation and its electrorheology, Microporous Mesoporous Mater. 93 (2006) 263–269.
[22] A. Mehdinia, M. Ovais Aziz-Zanjani, M. Ahmadifar, A. Jabbari, Design and synthesis of molecularly imprinted polypyrrole based on nanoreactor SBA-15 for recognition of ascorbic acid, Biosens. Bioelectron. 39 (2013) 88–93.
[23] F.F. Fang, H.J. Choi, W.S. Ahn, Electrorheology of a mesoporous silica having conducting polypyrrole inside expanded pores, Microporous Mesoporous Mater. 130 (2010) 338–343.
[24] M.S. Cho, H.J. Choi, K.Y. Kim, W.S. Ahn, Synthesis and characterization of polyaniline/mesoporous SBA-15 Nanocomposite, Macromol. Rapid Commun. 23 (2002) 713–716.
[25] D. Zhao, Q. Huo, J. Feng, B.F. Chmelka, G.D. Stucky, Nonionic triblock and star diblock copolymer and oligomeric surfactant syntheses of highly ordered, hydrothermally stable, mesoporous silica structures, J. Am. Chem. Soc. 120 (1998) 6024–6036.
[26] Q.Y.D.Y. Gao Xu Wu Sun, Adsorption of amino acids on SBA-15-type mesoporous materials, The 40th Anniversary of International Zeolites to Porous MOF Materials (2007) 961–965.

[27] Q. Tao, Zh. Xu, J. Wang, F. Liu, H. Wan, Sh. Zheng, Adsorption of humic acid to aminopropyl functionalized SBA-15, Microporous Mesoporous Mater. 131 (2010) 177–185.
[28] S.A. Idris, C.M. Davidson, C. Mc Manamon, M.A. Morris, P. Anderson, L.T. Gibson, Large pore diameter MCM-41 and its application for lead removal from aqueous media, J. Hazard. Mater. 185 (2011) 898–904.
[29] N. Ballav, A. Maity, Sh B. Mishra, High efficient removal of chromium (VI) using glycine doped polypyrrole adsorbent from aqueous solution, Chem. Eng. J. 198–199 (2012) 536–546.
[30] M. Arshadi, Manganese chloride nanoparticles: a practical adsorbent for the sequestration of Hg (II) ions from aqueous solution, Chem. Eng. J. 259 (2015) 170–182.
[31] B. Kakavandi, et al., Enhanced chromium (VI) removal using activated carbon modified by zero valent iron and silver bimetallic nanoparticles, J. Environ. Health Sci. Eng. 12 (2014) 115.
[32] E.P. Giannelis, Polymer-layered silicate nanocomposites: synthesis, properties and applications, Appl. Organomet. Chem. 12 (1998) 675–680.
[33] Sh.Ho Y-, T.-H. Chiang, Y.-M. Hsueh, Removal of basic dye from aqueous solution using tree fern as a biosorbent, Process Biochem. 40 (2005) 119–124.
[34] S. Shahmohammadi-Kalalagh, H. Babazadeh, A.H. Nazemi, M. Manshouri, Isotherm and kinetic studies on adsorption of Pb, Zn and Cu by kaolinite, Caspian J. Environ. Sci. 9 (2011) 243–255.
[35] H. Aghayan, A.R. Khanchi, A.R. Mahjoub, Synthesis and characterization of cesium molybdo vanado phosphate immobilized on platelet SBA-15: an efficient inorganic composite ion-exchanger for gadolinium ion sorption, Appl. Surf. Sci. 274 (2013) 7–14.
[36] K. Yaghmaeian, R. Khosravi Mashizi, S. Nasseri, A.H. Mahvi, M. Alimohammadi, S. Nazmara, Removal of inorganic mercury from aquatic environments by multi-walled carbon nanotubes, J. Environ. Health Sci. Eng. 13 (2015) 1–9 55.
[37] M. Zabihi, A. Ahmadpour, A. Haghighi Asl, Removal of mercury from water by carbonaceous sorbents derived from walnut Shell, J. Hazard. Mater. 167 (2009) 230–236.
[38] W.J. Weber, J.C. Morris, Kinetics of adsorption on carbon from solution, J. Sanit. Eng. Div. 89 (2) (1963) 31–60.
[39] H. El Boujaady, M. Mourabet, M. Bennani-Ziatni, A. Taitai, Adsorption/desorption of direct yellow 28 on apatitic phosphate: mechanism, kinetic and thermodynamic studies, J. Assoc. Arab Univ. Basic Appl. Sci. 16 (2014) 64–73.